

*Journal of*  
***Mechanics of***  
***Materials and Structures***

**FINITE ELEMENT SIMULATION OF STRAIN RATE EFFECTS ON  
LOCALIZED UNSTABLE PSEUDOELASTIC RESPONSE OF  
SHAPE MEMORY ALLOYS**

B. Azadi Borujeni, Daan M. Maijer and R. K. Nimal D. Rajapakse

***Volume 3, N° 10***

***December 2008***



## FINITE ELEMENT SIMULATION OF STRAIN RATE EFFECTS ON LOCALIZED UNSTABLE PSEUDOELASTIC RESPONSE OF SHAPE MEMORY ALLOYS

B. AZADI BORUJENI, DAAN M. MAIJER AND R. K. NIMAL D. RAJAPAKSE

A macromechanical total-deformation constitutive model of pseudoelasticity previously developed by the authors is employed within a two-dimensional finite element framework to numerically investigate the effect of strain rate and boundary conditions on the overall mechanical response and nucleation/evolution of transformation bands in NiTi strips during both forward and reverse transformations. The simulation results are compared with the experimental observations previously reported by other researchers, and it is shown that the present method successfully captures the nucleation and propagation of localized deformation bands during both loading and unloading. It is confirmed that the number of propagating fronts plays a key role in the pseudoelastic response of material in nonisothermal conditions. Special attention is paid to the morphology of the transformation fronts and its evolution. The numerical analysis indicates that the predicted morphology of the fronts is highly sensitive to imperfections and misalignments in the boundary conditions, especially during the reverse transformation.

### 1. Introduction

Owing to their unique mechanical properties, shape memory alloys (SMA) are increasingly being used in many engineering applications such as medical devices, orthodontic wires, microactuators, and vibration control [Otsuka and Wayman 1998; Saadat et al. 2002; Kohl 2004]. The two important characteristics of SMAs are known as *pseudoelasticity* (or *superelasticity*) and *shape memory effect*, which take place over different temperature ranges.

Despite extensive experimental and theoretical research in the past two decades, some aspects of SMA behavior are still subject to intense research. Among these are the instability of the mechanical behavior in some SMAs which leads to macroscale deformation localization (Lüders-like deformation) and sensitivity of their response to loading rate. It has been observed that at low strain rates, the uniaxial pseudoelastic response of NiTi is characterized by a distinct stress plateau and propagation of only one or two transformation fronts. At high strain rates, on the other hand, the stress-strain response maintains a positive slope, and multiple propagating fronts may coexist. Lüders-like deformation in NiTi was first observed by Miyazaki et al. [1981] in wire samples. The subject has been systematically studied through in-situ monitoring of the local variations of temperature and strain by Leo et al. [1993] and Shaw and Kyriakides [1995] in NiTi wires, by Shaw and Kyriakides [1997a] and Pieczyska et al. [2006a] in NiTi strips, and also recently by Feng and Sun [2006] in NiTi microtubes.

---

*Keywords:* shape memory alloys, strain rate, localization, phase transformation, pseudoelasticity, martensite reorientation, finite element method.

Various hypotheses have been proposed for the origin of deformation localization in NiTi. Some believe that the severe geometric distortion due to large transformation strain is the only cause for localization. In their view, the stress-strain curve maintains a positive (but small) slope during the transformation [Favier et al. 2002; Sittner et al. 2005]. Other researchers have attributed the deformation localization in NiTi to the intrinsic instability of the material behavior (strain softening) during the phase transformation [Shaw and Kyriakides 1997b; Idesman et al. 2005; Feng and Sun 2006]. This argument is supported by the fact that the large stress drop at the onset of the stress-plateau can not be modeled by geometric instability alone [Shaw and Kyriakides 1997b]. As shown by Iadicola and Shaw [2002], the “real” load drop can be as high as 17% if the stress concentrations at the gripped ends are eliminated.

Regardless of its origin, the localization of deformation in SMAs and its strong rate-dependency can place serious limitations on engineers who wish to design parts made of SMAs and exploit pseudoelastic properties. Therefore, a reliable and easy-to-use thermomechanical constitutive model is desired to enable engineers to predict the local and bulk material response.

Most of the constitutive models developed in the past have focused on the overall response of SMAs which exhibit stable mechanical behavior. Some examples of these models can be found in [Tanaka et al. 1986; Brinson 1993; Boyd and Lagoudas 1994; Lagoudas et al. 1996; Auricchio et al. 1997; Raniecki and LExcellent 1998; Brocca et al. 2002]. Although these models are often based on detailed thermodynamic considerations, their ability to model the unstable mechanical behavior is not guaranteed. It has been shown through numerical simulations that the ability of a constitutive model to successfully capture the stable pseudoelastic behavior does not automatically ensure the full recovery of inelastic deformation throughout the entire domain during the unstable localized reverse transformation [Azadi et al. 2007; Azadi 2008].

Abeyaratne and Knowles [1993] developed a one-dimensional thermodynamic framework based on the Helmholtz free energy to simulate the isothermal transformation in an SMA bar. The propagating phase boundaries were treated as traveling field discontinuities. Shaw and Kyriakides [1997b] proposed a model based on incremental plasticity to capture the material instability observed in NiTi strips. The material was assumed to behave as an isothermal, rate-independent  $J_2$ -type elasto-plastic solid with isotropic softening. A similar approach has also been recently used by Hu et al. [2007] to simulate the nucleation and propagation of localized helical bands in NiTi tubes. This analysis was extended in [Shaw 2000; Iadicola and Shaw 2004] by considering the thermomechanical coupling of the material with its environment, and investigated the effect of loading rate on the evolution of instabilities. Due to the irreversibility of plastic deformation, the use of incremental plasticity in these models is limited to the forward transformation case, and the reverse transformation upon unloading has been ignored.

Recently, Azadi et al. [2006] developed a one-dimensional phenomenological model to simulate the phase transformation and transformation front propagation in SMA wires. They assumed that the untransformed particles located close to the transformed regions are less stable than those away from the transformed regions. Azadi et al. [2007] extended the one-dimensional model to a multidimensional macromechanical model of localized unstable pseudoelasticity based on the deformation theory of plasticity. In this model, the finite form of transformation strain is expressed in terms of the gradient of a potential function, which allows for the reorientation of the transformation strain tensor with variation of the stress tensor, regardless of the occurrence of a phase transformation. The model is in fact similar to that proposed by Auricchio and Stefanelli [2004], although they did not consider the localization

phenomena and instability of mechanical behavior. Moreover, in the model of Azadi et al. [2007] the effect of temperature and variation of elastic properties upon phase transformation have also been considered. The constitutive model was successfully implemented within a finite element (FE) framework to simulate the isothermal nucleation and propagation of a single transformation front during the reverse transformations, as well as the forward transformation in a short NiTi strip. However, the simulation results were compared with the experimental data only for the forward transformation case. In the present work, the multidimensional analysis of Azadi et al. [2007] is extended to simulate the nucleation and propagation of multiple transformation fronts in longer strips of NiTi by considering the effect of heat generation/consumption occurring during the transformation, and thus the strain rate effects. Moreover, the simulation results are compared with experimental observations for both the forward and reverse transformations, which allows for a better assessment of the performance of the constitutive model. The effect of boundary conditions on the evolution of transformation bands morphology in NiTi strips is also investigated.

## 2. Constitutive model

A simple macromechanical constitutive model previously developed by Azadi et al. [2007] is used to model the pseudoelastic behavior of polycrystalline NiTi. The constitutive model is inspired by the deformation theory of plasticity, with two sets of yielding criteria for forward and reverse transformations. The model is intended to describe conditions at a local material point subjected to general thermomechanical loading. The equations governing the stress-strain relations and kinetics of transformations from Azadi et al. [2007] are summarized in Table 1. In these equations,  $\varepsilon_{ij}$  is the total strain tensor,  $\sigma_{ij}$  is the stress tensor,  $S_{ij}$  is the deviatoric stress tensor,  $\bar{\sigma}$  is the von Mises effective stress, and  $\gamma$  is the volume fraction

Constitutive Relations	Kinetic Relations
<p><b>Finite form:</b></p> $\varepsilon_{ij} = D_{ijkl}(\gamma) \sigma_{kl} + \frac{3}{2} \Delta \varepsilon_t (S_{ij} / \bar{\sigma}) \gamma,$ <p>where</p> $D_{ijkl}(\gamma) = \gamma D_{ijkl}^{(M)} + (1 - \gamma) D_{ijkl}^{(A)}.$ <p><b>Incremental form:</b></p> $d\varepsilon_{ij} = \bar{D}_{ijkl}(\gamma) d\sigma_{kl} + \left( (D_{ijkl}^{(M)} - D_{ijkl}^{(A)}) \sigma_{kl} + \frac{3}{2} \Delta \varepsilon_t \frac{S_{ij}}{\bar{\sigma}} \right) d\gamma,$ <p>where</p> $\bar{D}_{ijkl}(\gamma) = D_{ijkl}(\gamma) + \frac{3}{2} \frac{\Delta \varepsilon_t}{\bar{\sigma}} \left( \delta_{ik} \delta_{jl} - \frac{1}{3} \delta_{ij} \delta_{kl} - \frac{3}{2} \frac{S_{ij} S_{kl}}{\bar{\sigma}^2} \right) \gamma.$	<p><b>Forward transformation (<math>d\gamma &gt; 0, \gamma &lt; 1</math>):</b></p> $F_{A \rightarrow M}(\sigma_{ij}, \gamma, T) = 0, \quad dF_{A \rightarrow M} = 0,$ <p>where</p> $F_{A \rightarrow M} = \bar{\sigma} - (1 - \gamma) \sigma_{MN}(T) - \gamma \sigma_{MC}(T).$ <p><b>Reverse transformation (<math>d\gamma &lt; 0, \gamma &gt; 0</math>):</b></p> $F_{M \rightarrow A}(\sigma_{ij}, \gamma, T) = 0, \quad dF_{M \rightarrow A} = 0$ <p>where</p> $F_{M \rightarrow A} = \bar{\sigma} - \gamma \sigma_{AN}(T) - (1 - \gamma) \sigma_{AC}(T).$

**Table 1.** Summary of the constitutive model.

of martensite;  $D_{ijkl}^{(A)}$  and  $D_{ijkl}^{(M)}$  are the elastic compliances of the pure austenite and martensite phases, respectively, and  $\Delta\varepsilon_t$  is a material parameter, representing the maximum transformation strain that can be achieved during a uniaxial test.

The kinetics of phase transformation in the forward or reverse directions are controlled by a set of yield functions called *martensite nucleation stress* ( $\sigma_{MN}$ ), *martensite completion stress* ( $\sigma_{MC}$ ), *austenite nucleation stress* ( $\sigma_{AN}$ ), and *austenite completion stress* ( $\sigma_{AC}$ ). For materials such as NiTi, which exhibit localization of deformation and unstable mechanical behavior, the nucleation stress is higher (lower) than the completion stress during the forward (reverse) transformation. These critical values are temperature-dependent material properties and must be determined through a carefully designed and executed testing setup; see [Iadicola and Shaw 2002], for example.

The heat generation/consumption during the transformation is considered to be a result of inelastic work and enthalpy change due to phase transformation [Shaw 2000]. Therefore, the heat generation may be calculated as

$$\dot{q}_G = (\sigma_{ij}\dot{\varepsilon}_{ij} - \dot{u}^{(e)}) - \dot{h}. \quad (1)$$

In this equation,  $q_G$  is the generated heat,  $u^{(e)}$  is the elastic energy density, and  $\dot{h}$  is the enthalpy change. The elastic energy density is given by

$$u^{(e)} = \frac{1}{2}\sigma_{ij}\varepsilon_{ij}^{(e)}, \quad (2)$$

where  $\varepsilon_{ij}^{(e)}$  is the elastic part of the strain given by ([Azadi et al. 2007])

$$\varepsilon_{ij}^{(e)} = (\gamma D_{ijkl}^{(M)} + (1 - \gamma) D_{ijkl}^{(A)}) \sigma_{kl}. \quad (3)$$

It is assumed that the rate of change in enthalpy,  $\dot{h}$ , can be approximated by

$$\dot{h} = \begin{cases} \rho \Delta h_{A \rightarrow M} \dot{\gamma} & \text{if } \dot{\gamma} > 0, \\ -\rho \Delta h_{M \rightarrow A} \dot{\gamma} & \text{if } \dot{\gamma} < 0. \end{cases} \quad (4)$$

where  $\rho$  is the density and  $\Delta h_{A \rightarrow M}$ ,  $\Delta h_{M \rightarrow A}$  are the total changes in enthalpy per unit mass during the forward and reverse transformations at zero-stress. These quantities can be measured by differential scanning calorimetry (DSC). From Table 1 and equations (1) through (4), the heat generation term is obtained as

$$\dot{q}_G = \begin{cases} (\bar{\sigma} \Delta\varepsilon_t + \frac{1}{2}\sigma_{ij}(D_{ijkl}^{(M)} - D_{ijkl}^{(A)})\sigma_{kl} - \rho \Delta h_{A \rightarrow M})\dot{\gamma} & \text{if } \dot{\gamma} > 0, \\ (\bar{\sigma} \Delta\varepsilon_t + \frac{1}{2}\sigma_{ij}(D_{ijkl}^{(M)} - D_{ijkl}^{(A)})\sigma_{kl} + \rho \Delta h_{M \rightarrow A})\dot{\gamma} & \text{if } \dot{\gamma} < 0. \end{cases} \quad (5)$$

A few comments regarding the limitations and validity of the assumptions in this constitutive model are necessary. The current constitutive model is an extension of a mechanical theory (deformation theory of plasticity). Although the model is not derived from explicit thermodynamic considerations, it accounts for the hysteresis behavior and the proper direction of phase transformations and corresponding heat generation terms during loading and unloading, as validated by comparison with experiments. Nevertheless, the reformulation of the proposed constitutive theory in a consistent thermodynamic framework seems to be difficult.

The use of the von Mises effective stress in the yield criteria limits the application of the constitutive model to materials that behave symmetrically under tension and compression. As shown experimentally

(see [Liu et al. 1998], for example), NiTi alloys exhibit tension-compression asymmetry. The tension-compression asymmetry, however, does not impact the current work, which focuses on tension.

It has been shown through experiment that the phase transformation in NiTi may start homogeneously prior to the nucleation of localized deformation bands [Feng and Sun 2006; Daly et al. 2007]. Tan et al. [2004] also reported that the end of the stress plateau in the pseudoelastic response is not the end of the phase transformation, and that the stress-induced transformation continues beyond the stress plateau. The mechanically stable stress-induced phase transformation is not considered in this current analysis. However, it would be straightforward to incorporate into the constitutive model by revising the yield functions  $F_{A \rightarrow M}$  and  $F_{M \rightarrow A}$  in Table 1.

### 3. Numerical simulations

The constitutive model has been implemented within a FEM framework to predict the nucleation and propagation of transformation-induced instabilities during the pseudoelastic response of NiTi dog-bone samples at various strain rates. The simulations were run with the aid of an in-house FEM code developed by the authors. The geometry of the sample and FE mesh are shown in Figure 1, left. The sample

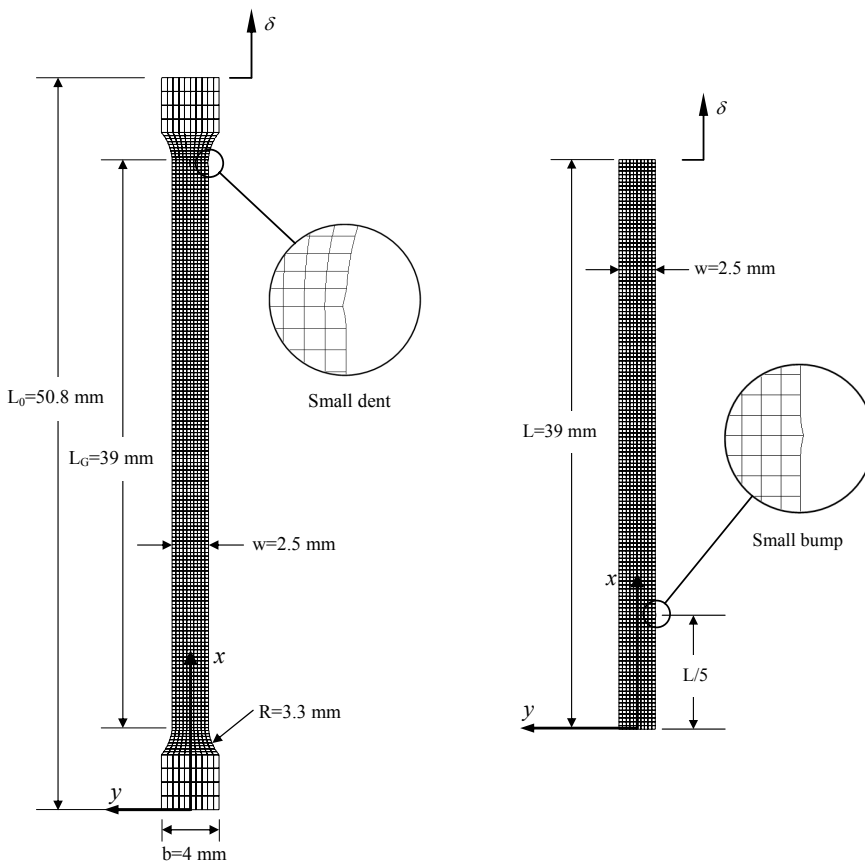


**Figure 1.** Left: Geometry and finite element discretization of the sample. Right: Geometry and mesh used for calibration of the model in reverse transformation.

dimensions are based on the dog-bone sample used in the experiments of Shaw and Kyriakides [1997a], which has a uniform thickness of 0.4 mm. The two-dimensional spatial domain was discretized with 8-node Serendipity plane-stress elements. The gauge section was discretized with 150 elements along the length and 10 elements across the width. A small dent with a depth of 0.04 mm was introduced at the top right corner of the gauge section as shown in the figure. The purpose of this geometric imperfection was to control the location of the first nucleation.

The nodal displacements along the bottom end of the specimen ( $x = 0$ ) are fixed while those across the top end ( $x = L_0$ ) are pulled at a constant rate. The temperatures of both ends are fixed at the ambient temperature (25 °C). Shaw [2000] rationalized this assumption based on the large size of the metallic grips used in the experiments. The heat loss due to natural convection has been considered by assuming a constant convective film coefficient,  $h_{\text{conv}} = 4 \text{ W/m}^2 \text{ K}$ , for all the exposed surfaces and free edges of the sample [Shaw 2000]. The imposed mechanical and thermal boundary conditions are expressed as

$$\begin{aligned} u|_{x=0} = 0, \quad v|_{x=0,y=0} = 0, \quad T|_{x=0} = 25^\circ\text{C}, \quad \dot{q}|_{\text{surface}} = h_{\text{conv}}(T - 25^\circ\text{C}), \\ u|_{x=L_0} = \delta, \quad v|_{x=L_0,y=0} = 0, \quad T|_{x=L_0} = 25^\circ\text{C}, \quad \dot{q}|_{\text{edge}} = h_{\text{conv}}(T - 25^\circ\text{C}), \end{aligned} \quad (6)$$

where  $u$  and  $v$  are the displacement components in the  $x$ - and  $y$ -directions, respectively,  $\delta$  is the applied end displacement,  $T$  (°C) is the temperature, and  $\dot{q}$  ( $\text{W/m}^2$ ) is the rate of heat loss per unit area.

In the experiments of Shaw and Kyriakides [1997a], the variation in temperature at the moderate strain rate was in the range of +12°C and –5°C. Therefore, heat transfer through radiation was assumed to be negligible. Thermal expansion/contraction was also ignored in the following analysis due to its minor effect on the results.

The sensitivity of the present numerical analysis to mesh size, and the uniqueness of the solution were examined by the authors. Despite the instability of mechanical behavior, only minor mesh sensitivity was observed in the numerical simulations conducted with finer meshes. As pointed out by Shaw [2000], the generation or absorption of heat during the transformation stabilizes the mechanical response. Additionally, the recovery of material stability at the end of phase transformation has an overall stabilizing effect on the solution. As a result, the overall force-displacement response, temperature variation, the number of nucleation events, and the basic features of the front morphology are not affected by mesh size. However, the exact location and timing of nucleation events, and also the orientation of transformation bands ( $+\theta$  or  $-\theta$ ) are sensitive to numerical noise.

In the following subsections, the model is first calibrated using data from “isothermal” experiments performed at various temperatures, and then implemented to simulate the “nonisothermal” responses of the specimen at various strain rates.

**3A. Material parameters and calibration of the constitutive model.** We assume in our analysis that individual solid phases behave as isotropic materials. A set of stress-strain curves derived from the isothermal uniaxial tensile tests on NiTi dog-bone samples reported by Shaw [2000] have been used to find the mechanical parameters of the constitutive model. The mechanical responses of the material at three different temperatures (15, 25, and 35 °C) have been considered for this purpose. The elastic modulus of individual phases ( $E_A$ ,  $E_M$ ), and the transformation strain ( $\Delta\varepsilon_l$ ) are the average values measured directly from the experimental results.

In order to find the nucleation and completion stresses during the forward transformation, a set of isothermal simulations at various temperatures were run on the dog-bone sample shown in Figure 1, left. By best fitting the nominal nucleation stress and propagation stress (Maxwell stress) obtained from the numerical analysis to those from the experiments at the above mentioned temperatures, the following linear relationships were established:

$$\begin{aligned}\sigma_{\text{MN}}(T) &= 9.4258 T + 189.13 && \text{(MPa)}, \\ \sigma_{\text{MC}}(T) &= 4.8158 T + 232.73 && \text{(MPa)}.\end{aligned}\tag{7}$$

The tapered sections of the sample in Figure 1 experience a lower level of stress. Therefore, some residual austenite remains in those areas at the end of the stress plateau. This effect masks a visible stress valley at the onset of the reverse transformation in the stress-strain response, both in the simulations and experiments. In order to eliminate the end effects, Shaw and Kyriakides [1997a] used straight specimens to measure the nucleation stress during the reverse transformation. During these tests, austenite nucleation upon unloading occurs in the middle of the test section and is accompanied by a distinct stress valley. To calibrate the model for the reverse transformation, a straight specimen was also used in the isothermal simulations, as depicted in Figure 1, right. The dimensions and FE mesh of the specimen are similar to those of the gauge section of the dog-bone sample. A slight side imperfection in the form of a bump was introduced at  $x=L/5$  to control the location of the first nucleation (Figure 1, right). The height of the bump was 0.04 mm. The specimen was first loaded until the entire domain was fully transformed into martensite, and then was unloaded.

The following linear relationships were found to best fit the nucleation and propagation stresses of the reverse transformation obtained from the isothermal experiments at different temperatures,

$$\begin{aligned}\sigma_{\text{AN}}(T) &= 7.5128 T - 44.22 && \text{(MPa)}, \\ \sigma_{\text{AC}}(T) &= 10.276 T - 35.31 && \text{(MPa)}.\end{aligned}\tag{8}$$

In equations (7) and (8), the temperature is in °C, and stresses are the second Piola–Kirchhoff stresses (Green strains and second Piola–Kirchhoff stresses were employed in the FE formulation in anticipation of future research). The variation of the nucleation and completion stresses with temperature is shown in Figure 2. In this figure, the nominal (engineering) nucleation and propagation stresses as determined by the isothermal simulations are also shown. There is a large difference between the engineering nucleation stress and the second Piola–Kirchhoff nucleation stress during the reverse transformation, which is due to the large amount of strain induced during the forward transformation. In order to show the close fit of the chosen mechanical properties, the overall pseudoelastic responses of the dog-bone sample based on the isothermal simulations are compared to the experimental results in Figure 3.

Thermal parameters of the NiTi strip, including zero-stress enthalpy change,  $\Delta h_{\text{A}\rightarrow\text{M}}$ , the thermal conductivity,  $k$ , specific heat capacity,  $C_p$ , and density,  $\rho$ , were taken from [Shaw 2000]. It was also assumed that the stress-free enthalpy change for the martensite to austenite transformation,  $\Delta h_{\text{M}\rightarrow\text{A}}$ , is the negative of that for the austenite to martensite transformation. As an approximation, all thermal parameters were assumed to be independent of phase, temperature, or other state variables. Table 2 summarizes the chosen mechanical and thermal properties.

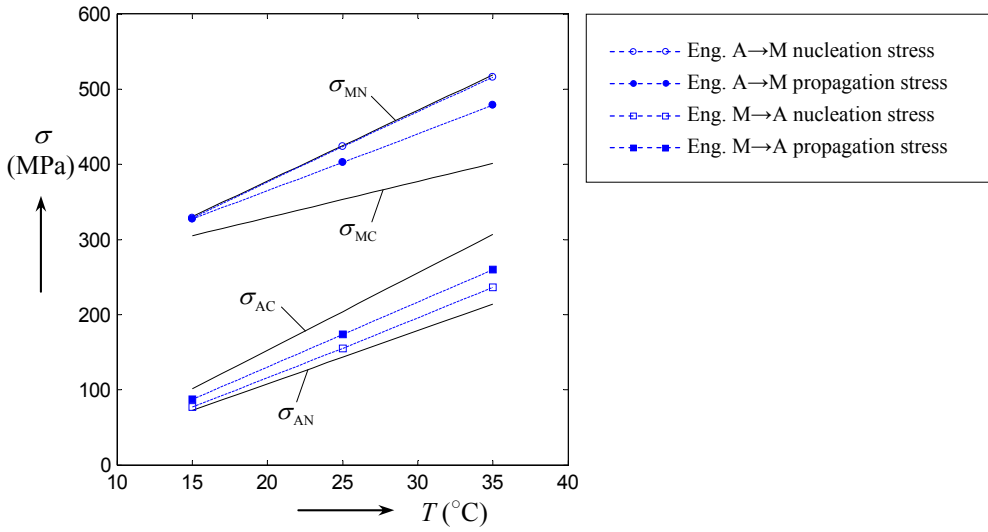


**Figure 2.** Chosen second Piola–Kirchhoff nucleation and completion stresses, and corresponding engineering values calculated from the isothermal simulations.

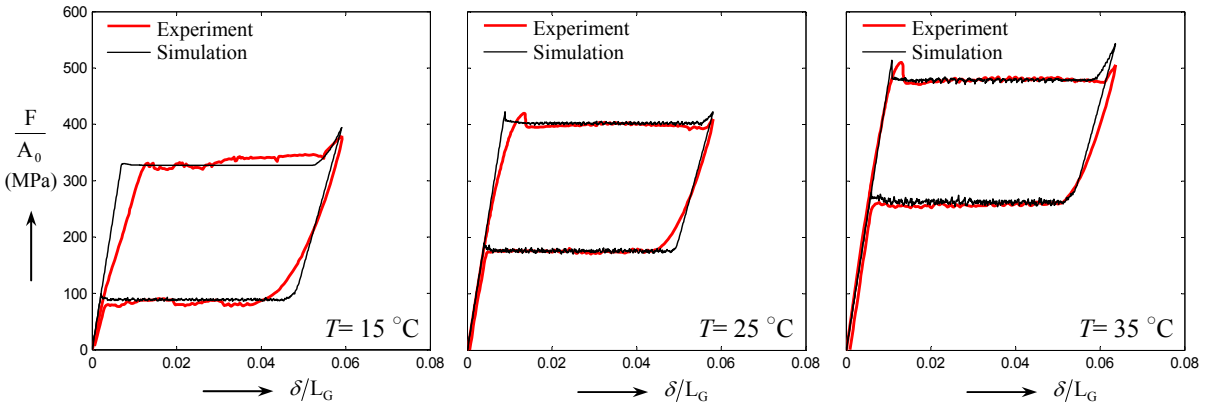


**Figure 3.** Pseudoelastic response of NiTi strip under isothermal conditions at different temperatures. Experimental curves are adapted from [Shaw 2000].

**3B. Simulation of loading-unloading at low strain rate.** The pseudoelastic response of the dog-bone sample shown in Figure 1 was simulated for low strain rate displacement-controlled loading-unloading. The ambient air temperature surrounding the sample and the temperature of the grips was 25 °C. The specimen was loaded at a constant rate of  $\dot{\delta}/L_G = 10^{-4} \text{ s}^{-1}$ . The deformation was paused at  $\delta/L_G = 6.4 \%$  for 5 minutes to allow the sample to reach thermal equilibrium, followed by unloading at a constant rate of  $\dot{\delta}/L_G = -10^{-4} \text{ s}^{-1}$ . The predicted force-displacement response is compared with the experimental measurements of Shaw and Kyriakides [1997a] in Figure 4. A sequence of 14 contour graphs showing the distribution of phase and temperature corresponding to the deformed configurations of the specimen during the forward transformation are provided in Figure 5. The contours are separated by intervals of  $\delta/L_G = 0.4 \%$  with the first and last contour corresponding to  $\delta/L_G = 0.8 \%$  and  $\delta/L_G = 6 \%$ , respectively.

Parameter		Value
Elastic modulus of Austenite	$E_A$ (GPa)	57.55
Elastic modulus of Martensite	$E_M$ (GPa)	28.00
Poisson's ratio	$\nu_A, \nu_M$	0.3
Transformation strain	$\Delta \varepsilon_t$	0.0429
Martensite nucleation stress	$\sigma_{MN}$ (MPa)	$9.4258 T(^{\circ}C) + 189.13$
Martensite completion stress	$\sigma_{MC}$ (MPa)	$4.8158 T(^{\circ}C) + 232.73$
Austenite nucleation stress	$\sigma_{AN}$ (MPa)	$7.5128 T(^{\circ}C) - 44.22$
Austenite completion stress	$\sigma_{AC}$ (MPa)	$10.276 T(^{\circ}C) - 35.31$
Enthalpy change at zero-stress	$\Delta h_{A \rightarrow M}, -\Delta h_{M \rightarrow A}$ (J kg <sup>-1</sup> )	$-12.3 \times 10^3$
Thermal conduction coefficient	$k$ (W m <sup>-1</sup> K <sup>-1</sup> )	18
Specific heat capacity	$C_p$ (J kg <sup>-1</sup> K <sup>-1</sup> )	837
Density	$\rho$ (kg m <sup>-3</sup> )	$6.5 \times 10^3$

**Table 2.** Mechanical and thermal properties of the NiTi strip.

The first region to transform to martensite nucleates at the geometric imperfection described earlier, and a sharp inclined deformation band forms with the well-known angle of  $55^{\circ}$  to the specimen axis. Upon additional loading, the single, well-defined transformation front evolves into an alternating criss-cross pattern, which is similar to the pattern Shaw and Kyriakides [1997a] observed in their experiments. As loading continues, the temperature at the transformation front increases (Figure 5), which in turn results in an increase in the nominal stress as shown in Figure 4. At  $\delta/L_G \approx 2.7\%$ , a second transformation front nucleates at the lower end of the gauge section due to the stress concentration near the round fillet. The second nucleation event causes the drop in the load observed in both the experiment and the simulation results (refer to Figure 4). As the fronts approach each other, they become straight and inclined across the width with the same orientation to minimize the mismatch between them. At the instant of coalescence,

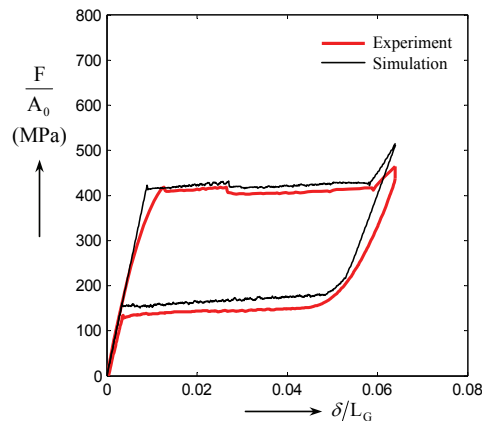


**Figure 4.** Pseudoelastic response of NiTi strip at  $\dot{\delta}/L_G = 10^{-4} \text{ s}^{-1}$ . The experimental response is adapted from Shaw and Kyriakides [1997a].

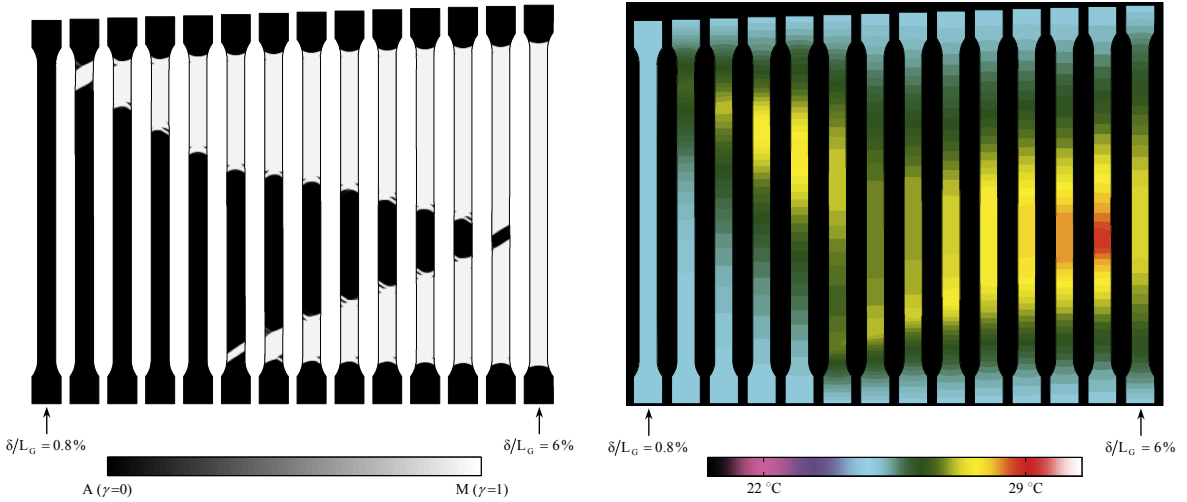


**Figure 5.** Sequence of events during  $A \rightarrow M$  transformation at  $\dot{\delta}/L_G = 10^{-4} \text{ s}^{-1}$ . Left: Martensitic fraction; right: Temperature.

the fronts make an angle of  $57.5^\circ$  with the loading axis. Overall, the mechanical response, distribution of temperature, evolution of transformation, and details of the transformation front are in good agreement with the experimental observations of Shaw and Kyriakides [1997a].

The sequence of events leading to the initial shape change of the transformation front is particularly interesting. Figure 6 shows a close up view of the transformation front (phase distribution contour) and distorted mesh. The lateral displacement ( $v$ ) has been multiplied by a factor of 20 to accentuate the lateral deflection in Figure 6, bottom. When the inclined transformation band nucleates at time 1 and begins to spread, the lateral deflection increases continuously at the front. The lateral deflection reaches its maximum between times 5 and 6, where the first finger emanates from the upper front in order to balance the lateral deflection and straighten the specimen. As a result, the lateral deflection decreases from times 6 to 8. The subsequent evolution of the transformation front can be described as successive nucleation and growth of finger patterns in alternative directions in order to keep the lateral deflection minimum.

During the pause between loading and unloading, the temperature of the sample equilibrates prior to returning to the ambient temperature. The evolution of the transformed phase and the temperature distribution during the reverse transformation are shown in Figure 7. As expected, the reverse transformation initiates at the tapered ends of the sample due to the reduced stress at these regions. The two transformation fronts propagate toward each other at the same speed. During most of the unloading part, the converging fronts are predicted to propagate through inverse shrinkage of the finger-type patterns observed during the forward transformation. However, experimental results of Shaw and Kyriakides [1997a] suggested that the fronts during the reverse transformation are quite sharp and straight with an inclination angle of approximately  $56^\circ$ . This discrepancy between the predicted and observed results is probably due to the lack of information on the exact boundary conditions at the gripped ends in the

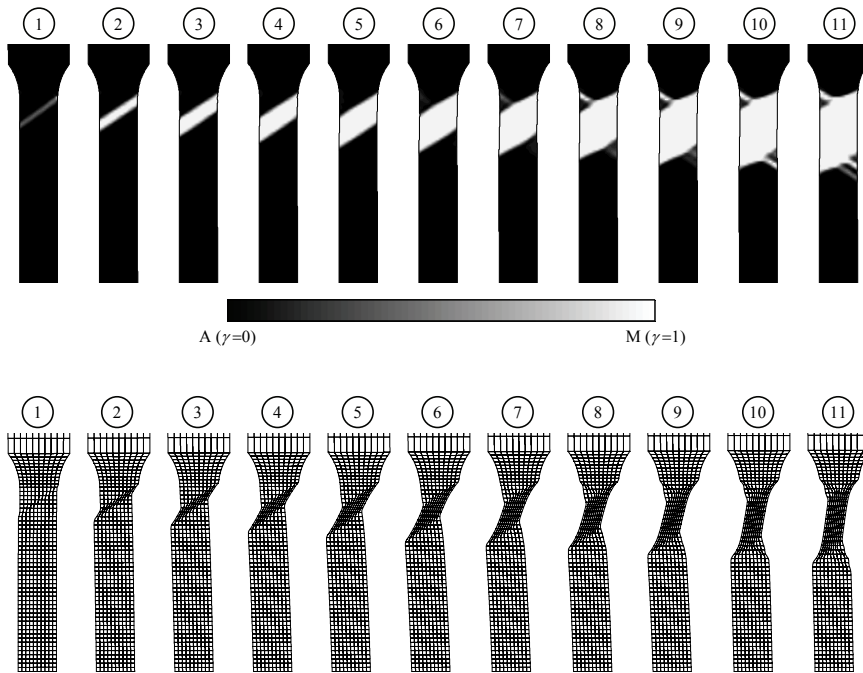


**Figure 6.** Details of front morphology evolution during  $A \rightarrow M$  transformation. Top: distribution of phases; bottom: distorted mesh with lateral displacement multiplied by a factor of 20.

experiment. As will be discussed later, small misalignments in the boundary conditions may result in sharp inclined fronts during the reverse transformation.

In addition to difference in the shape of the transformation front, the magnitude of the predicted temperature drop during the reverse transformation is also different from the measurements of Shaw and Kyriakides [1997a]. The maximum temperature drop observed during the experiment was  $-2^{\circ}\text{C}$ , whereas in the simulation it was predicted to reach  $-3.6^{\circ}\text{C}$ . This discrepancy may be partly due to uncertainties in the thermophysical properties of the specimen and thermal boundary conditions, and/or partly due to the assumption that the zero-stress latent heats associated with the forward and reverse transformations have the same value.

**3C. Simulation of loading-unloading at moderate strain rate.** The pseudoelastic response of the dog-bone SMA specimen was simulated for a moderate strain rate condition. A constant loading rate of  $\dot{\delta}/L_G = 10^{-3} \text{ s}^{-1}$  was applied until  $\delta/L_G = 7.65\%$ , followed by a 5 minute hold, then unloading at the same constant rate. The ambient air temperature was  $25^{\circ}\text{C}$ . The nominal stress-strain response is shown in Figure 8. The evolution of phase transformation and the distribution of temperature during the forward and reverse transformations are depicted in Figures 9 and 10. The transformation behavior is very similar to the experimental observations of Shaw and Kyriakides [1997a]. The localized transformation is first nucleated at the top corner, followed by a second nucleation event at the lower end, then two nucleation events in the mid span. The shape of transformation fronts match those observed in the experiment. For

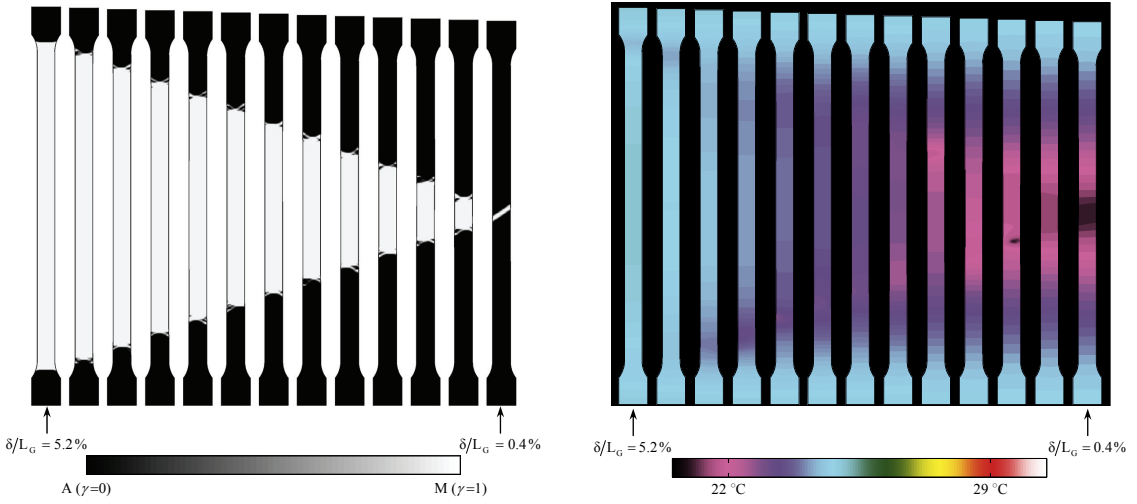


**Figure 7.** Sequence of events during  $M \rightarrow A$  transformation at  $\dot{\delta}/L_G = -10^{-4} \text{ s}^{-1}$ . Left: martensitic fraction; right: temperature.

the duration of the loading phase, they are sharp and straight, with an inclination angle ranging from  $55^\circ$  to  $65^\circ$  to the vertical axis. Only occasionally will one or two fingers develop at the front. This can be explained by noticing that the lateral deflection developed in each front compensate the lateral deflection in another front, and therefore the sharply inclined fronts can survive without branching and developing crossing fingers.

An interesting feature of the stress-strain response in Figure 8 is the stress-relaxation during the pause between loading and unloading, which can be seen in both the simulation and experimental results. This stress-relaxation is caused by the phase transformation due to the temperature decrease during the pause period [Pieczyska et al. 2006b].

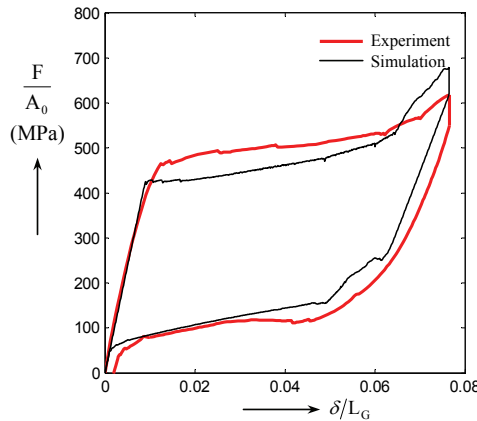


**Figure 8.** Pseudoelastic response of NiTi strip at  $\dot{\delta}/L_G = 10^{-3} \text{ s}^{-1}$ . Experimental data are from Shaw and Kyriakides [1997a].

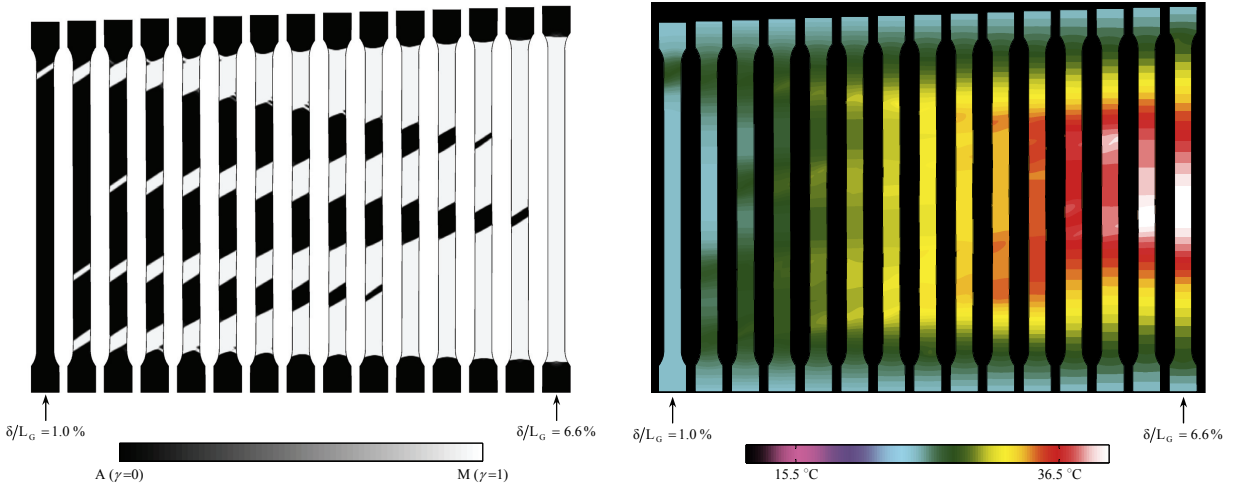


**Figure 9.** Sequence of events during forward transformation at  $\dot{\delta}/L_G = 10^{-3} \text{ s}^{-1}$ . Left: martensitic fraction; right: temperature.

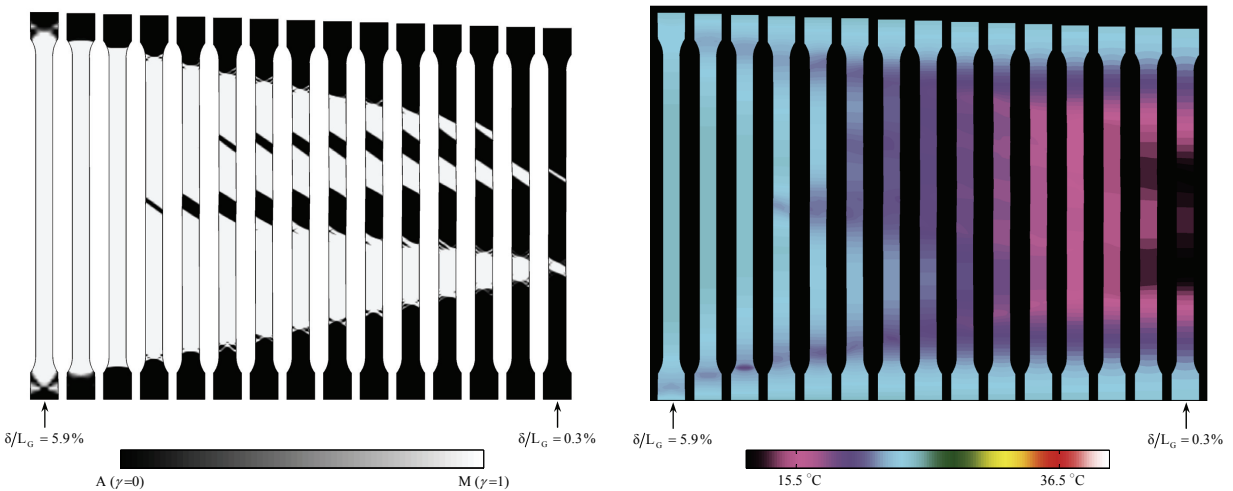


**Figure 10.** Sequence of events during reverse transformation at  $\dot{\delta}/L_G = -10^{-3} \text{ s}^{-1}$ . Left: martensitic fraction; right: temperature.

Unlike the low strain rate case, the transformation fronts during unloading at this moderate strain rate are mostly straight, with an inclination between  $54^\circ$  and  $62^\circ$ . The fronts emanating from the sample ends, however, are initially fingered and gradually become straight as they approach the middle fronts.

The temperature distributions during the forward transformation agree with the measurements of Shaw and Kyriakides [1997a]. However, as in the previous simulation, the predicted temperatures exhibit a much larger temperature drop ( $-13^\circ\text{C}$ ) during the reverse transformation as compared to the experiments ( $-5^\circ\text{C}$ ). This large deviation from the experimental measurements suggests that the stress-free enthalpy

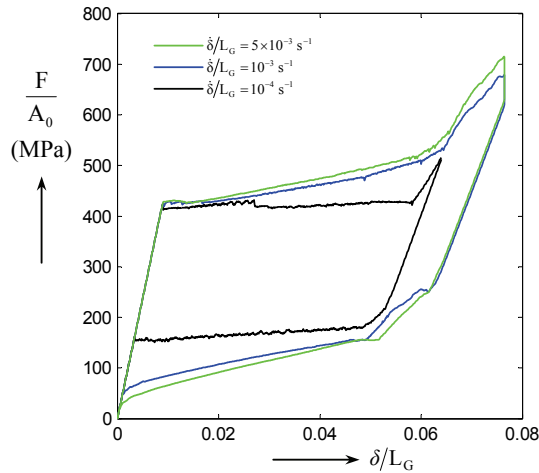


**Figure 11.** Simulated pseudoelastic response of NiTi strip at various elongation rates.

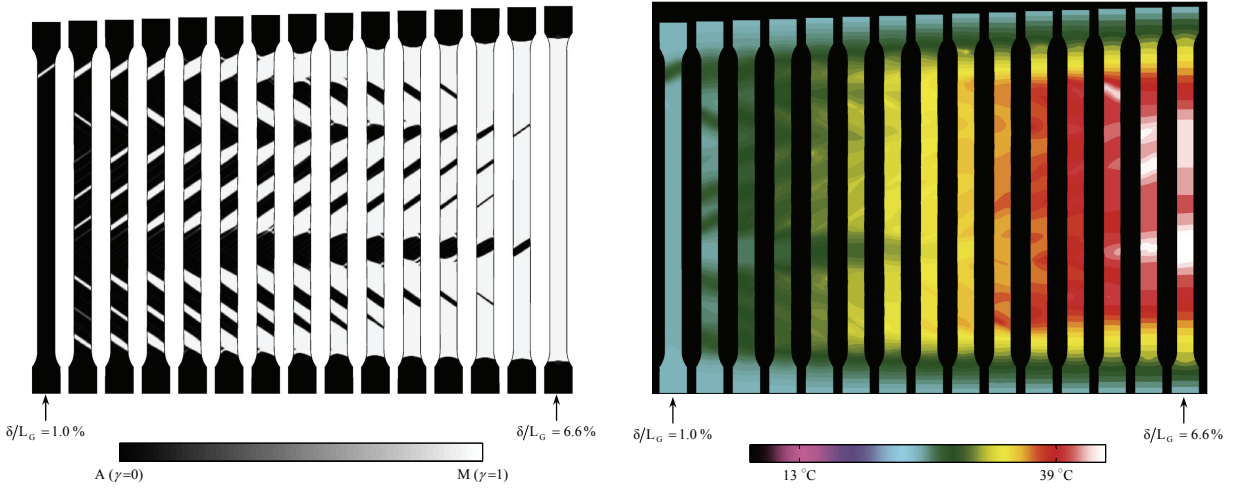
change during the reverse transformation ( $\Delta h_{M \rightarrow A}$ ) must be substantially smaller than its counterpart during the forward transformation. The DSC measurements reported in Shaw [2000], however, do not show such a large difference. Further investigation is needed to clarify this issue.

**3D. Simulation of loading-unloading at high strain rate.** The simulation was performed for a high strain rate beyond the loading rates applied in the experiments of Shaw and Kyriakides [1997a]. The elongation rate in this case was  $\dot{\delta}/L_G = 5 \times 10^{-3} \text{ s}^{-1}$ , which is five times faster than the moderate strain rate case. The loading was stopped at  $\delta/L_G = 7.65\%$ , followed by a 5 minute hold and subsequent unloading. The predicted nominal stress-strain response at this rate is compared to those at the low and moderate strain rates in Figure 11. The evolution of the phase transformations and temperature during loading and unloading are shown in Figures 12 and 13, respectively.

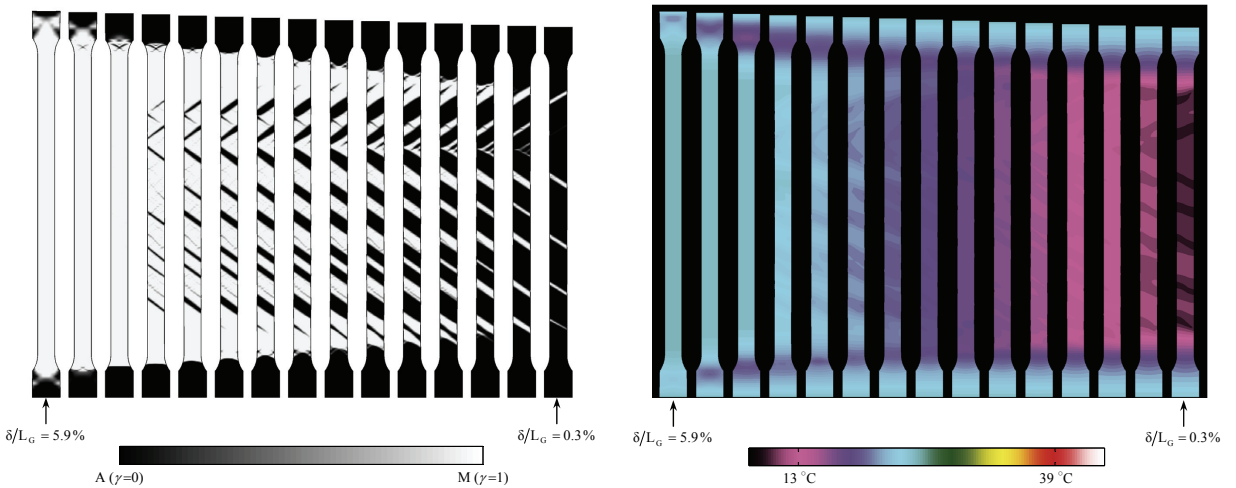
Similar to previous cases, the first nucleation event occurs at the top end of the gauge section where the geometric imperfection is located. Shortly after that, 7 narrow bands, some parallel and some opposing each other, are nucleated almost simultaneously in the gauge section. The number of nucleation events in this case is substantially larger than those observed in the previous two cases.

Figure 11 indicates that the change in the nominal stress-strain response with strain rate does not exhibit a linear trend. The difference between the stress-strain curves at the low and moderate strain rates is more pronounced than the difference between those at the moderate and high strain rates. As explained earlier, the increase or decrease in stress is caused by the increase or decrease in the temperature of transformation fronts. The magnitude of temperature variation at a front depends on the rate of transformation, which is proportional to the speed at which the transformation front propagates. On the other hand, the propagation speed decreases with the number of coexisting transformation fronts. Consequently, the increase of the transformation front temperature in the high strain rate case is hampered by the increase in the number of transformation fronts, which in turn results in a relatively small increase in the nominal stress.

By increasing the elongation rate, it is seen that the transformation fronts become even sharper, and emanating fingers disappear during the reverse transformation. This is due to the fact that the number



**Figure 12.** Sequence of events during forward transformation at  $\dot{\delta}/L_G = 5 \times 10^{-3} \text{ s}^{-1}$ . Left: martensitic fraction; right: temperature.



**Figure 13.** Sequence of events during reverse transformation at  $\dot{\delta}/L_G = -5 \times 10^{-3} \text{ s}^{-1}$ . Left: martensitic fraction; right: temperature.

of nucleation events increases by an increase in the strain rate. Concurrent transformation fronts help to maintain the overall straightness of the sample by cancelling each other. Hence, the sharp inclined transformation fronts survive for long periods before finally merging.

**3E. Effect of boundary conditions.** When performing uniaxial tension tests, it is important to minimize grip misalignment in order to reduce the out-of-axis loading. However, in practice, a pure uniaxial test may be difficult to achieve. For most materials which exhibit stable mechanical behavior, the small variation in loading conditions does not usually affect the observed behavior. But it is suspected that the

transformation behavior of NiTi samples undergoing uniaxial tensile tests may be sensitive due to the instability of the mechanical response. The dog-bone simulation has been used to evaluate the possible effects of misalignment on the transformation behavior. A lateral misalignment of 0.35 mm was applied to the lower end of the sample shown in Figure 1. The new displacement boundary conditions are now

$$\begin{aligned} u|_{x=0} &= 0, & v|_{x=0,y=0} &= 0.35 \text{ mm} \\ u|_{x=L_0} &= \delta, & v|_{x=L_0,y=0} &= 0. \end{aligned} \tag{9}$$

All other boundary conditions were applied as previously described. The simulations for the low and moderate strain rate conditions were repeated with new boundary conditions. The overall force-displacement response, the number of transformation fronts, and distribution of temperature were not affected by the new boundary conditions in any of the simulations. The only major change was observed in the morphology of the transformation fronts during the reverse transformation, especially at the low strain rate. Figure 14 shows the evolution of the reverse transformation in this case.

The two transformation fronts in Figure 14 become sharp and straight shortly after they exit the tapered ends of the specimen. As explained earlier, a straight inclined front tends to increase the amount of lateral deflection, which in turn helps to compensate for the misalignment of specimen ends. During the forward transformation, the large axial load acts as a restorative force opposing the growth of lateral deflection; thus the straight inclined fronts eventually convert to criss-cross fronts. During the reverse transformation, the transformation proceeds at a much smaller axial load, and therefore a larger amount of lateral deflection can exist. The kinking of the specimen due to lateral deflection is visible in Figure 14, which can also be observed in the experiments of Shaw and Kyriakides [1997a].

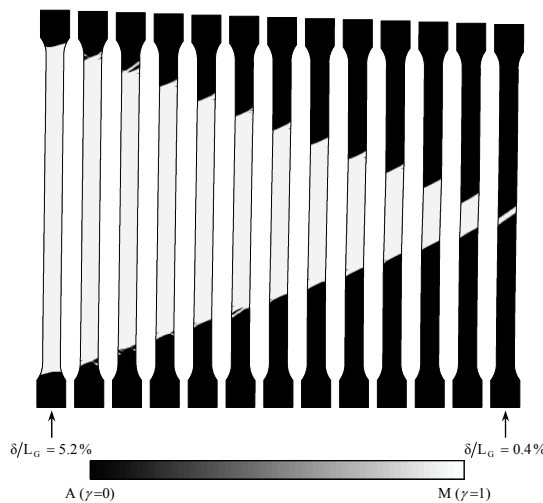


**Figure 14.** Transformation behavior of the specimen with misaligned grips during reverse transformation at  $\dot{\delta}/L_G = -10^{-4} \text{ s}^{-1}$ .

#### 4. Summary and conclusions

A numerical study of the nucleation and propagation of transformation bands during unstable pseudoelastic behavior of NiTi dog-bone samples has been presented. A multidimensional macroscopic constitutive model of SMA derived based on the deformation theory of plasticity was implemented within a two-dimensional finite element model to simulate the material response. Unlike similar numerical analyses in the past, the present model is able to capture the localization of transformation during unloading, as well as loading. The constitutive model was calibrated based on isothermal quasi-static uniaxial pseudoelastic experiments available in the literature. The thermomechanical coupling that occurs during the transformation, and the effect of loading rate on the overall mechanical response and evolution of a localized deformation were successfully simulated both during the forward and reverse transformations. The basic features of transformation front morphology and its evolution during forward and reverse transformations were also captured by the numerical analysis.

The following conclusions can be drawn based on the analysis presented in this paper:

- (1) The current macromechanical constitutive model's ability to correctly describe the forward and reverse transformations verifies that the continuum-level phenomena are the major players in the nucleation and propagation of martensitic transformation and its reverse transformation in NiTi shape memory alloys, regardless of the detailed microstructural root of the material instability.
- (2) The comparison between the calculated temperature drop during reverse transformation and experimental measurements clearly indicate that the zero-stress enthalpy change (stress-free latent heat) of the forward transformation must be greater than that of the reverse transformation. This conclusion, however, does not agree with the DSC measurements. Further experimental and theoretical analysis is required to clarify this difference.
- (3) The number of propagating transformation fronts is an important factor in determining the overall mechanical response of the material in nonisothermal conditions. The number of coexisting transformation fronts influences the local variations of temperature at individual fronts, which in turn affects the overall pseudoelastic response.
- (4) A small misalignment in the loading axis during uniaxial loading-unloading of a NiTi sample can dramatically affect the shape of transformation fronts during the reverse transformation. This is due to the lower stress level during the reverse transformation as compared to the forward transformation, which allows the specimen to develop kinks along its span.

The present methodology forms the basis of an analytical tool for use in analyzing SMA components subjected to various thermomechanical loading conditions within the unstable pseudoelastic regime.

#### References

- [Abeyaratne and Knowles 1993] R. Abeyaratne and J. K. Knowles, "Continuum model of a thermoelastic solid capable of undergoing phase transitions", *J. Mech. Phys. Solids* **41**:3 (1993), 541–571.
- [Auricchio and Stefanelli 2004] F. Auricchio and U. Stefanelli, "Numerical analysis of a three-dimensional super-elastic constitutive model", *Int. J. Numer. Methods Eng.* **61**:1 (2004), 142–155. MR 2005b:74100
- [Auricchio et al. 1997] F. Auricchio, R. Taylor, and J. Lubliner, "Shape-memory alloys: Macromodelling and numerical simulations of the superelastic behavior", *Comput. Methods Appl. Mech. Eng.* **146**:3–4 (1997), 281–312.

- [Azadi 2008] B. Azadi Borujeni, *Constitutive modelling and finite element analysis of the dynamic behavior of shape memory alloys*, Ph.D. dissertation, Department of Mechanical Engineering, University of British Columbia, Vancouver, 2008, Available at <https://circle.ubc.ca/handle/2429/796>.
- [Azadi et al. 2006] B. Azadi, R. K. N. D. Rajapakse, and D. M. Maijer, “One-dimensional thermomechanical model for dynamic pseudoelastic response of shape memory alloys”, *Smart Mater. Struct.* **15**:4 (2006), 996–1008.
- [Azadi et al. 2007] B. Azadi, R. K. N. D. Rajapakse, and D. M. Maijer, “Multi-dimensional constitutive modeling of SMA during unstable pseudoelastic behavior”, *Int. J. Solids Struct.* **44**:20 (2007), 6473–6490.
- [Boyd and Lagoudas 1994] J. Boyd and D. Lagoudas, “A constitutive model for simultaneous transformation and reorientation in shape memory materials”, pp. 159–177 in *Mechanics of phase transformations and shape memory alloys* (Chicago, 1994), edited by L. C. Brinson and B. Moran, AMD **189**, ASME, New York, 1994.
- [Brinson 1993] L. C. Brinson, “One-dimensional constitutive behavior of shape memory alloys: Thermomechanical derivation with non-constant material functions and redefined martensite internal variable”, *J. Intell. Mater. Syst. Struct.* **4**:2 (1993), 229–242.
- [Brocca et al. 2002] M. Brocca, L. C. Brinson, and Z. P. Bazant, “Three-dimensional constitutive model for shape memory alloys based on microplane model”, *J. Mech. Phys. Solids* **50**:5 (2002), 1051–1077.
- [Daly et al. 2007] S. Daly, G. Ravichandran, and K. Bhattacharya, “Stress-induced martensitic phase transformation in thin sheets of Nitinol”, *Acta Mater.* **55**:10 (2007), 3593–3600.
- [Favier et al. 2002] D. Favier, Y. Liu, L. Orgeas, and G. Rio, “Mechanical instability of NiTi in tension, compression and shear”, pp. 205–212 in *IUTAM Symposium on Mechanics of Martensitic Phase Transformation in Solids* (Hong Kong, 2001), edited by Q. P. Sun, Solid Mechanics and its Applications **101**, Kluwer, Dordrecht, 2002.
- [Feng and Sun 2006] P. Feng and Q. P. Sun, “Experimental investigation on macroscopic domain formation and evolution in polycrystalline NiTi microtubing under mechanical force”, *J. Mech. Phys. Solids* **54**:8 (2006), 1568–1603.
- [Hu et al. 2007] Z. Hu, Q. P. Sun, and Z. Zhong, “Numerical simulation for stress-induced phase transformation of SMAs tube under tension”, *Key Eng. Mat.* **340-341** (2007), 1181–1186.
- [Iadicola and Shaw 2002] M. A. Iadicola and J. A. Shaw, “An experimental setup for measuring unstable thermo-mechanical behavior of shape memory alloy wire”, *J. Intell. Mater. Syst. Struct.* **13**:2–3 (2002), 157–166.
- [Iadicola and Shaw 2004] M. A. Iadicola and J. A. Shaw, “Rate and thermal sensitivities of unstable transformation behavior in a shape memory alloy”, *Int. J. Plast.* **20**:4–5 (2004), 577–605.
- [Idesman et al. 2005] A. V. Idesman, V. I. Levitas, D. L. Preston, and J.-Y. Cho, “Finite element simulations of martensitic phase transitions and microstructures based on a strain softening model”, *J. Mech. Phys. Solids* **53**:3 (2005), 495–523. MR 2005h:74060
- [Kohl 2004] M. Kohl, *Shape memory microactuators*, Springer, Berlin, 2004.
- [Lagoudas et al. 1996] D. C. Lagoudas, Z. Bo, and M. A. Qidwai, “A unified thermodynamic constitutive model for SMA and finite element analysis of active metal matrix composites”, *Mech. Compos. Mater. Struct.* **3**:2 (1996), 153–179.
- [Leo et al. 1993] P. H. Leo, T. W. Shield, and O. P. Bruno, “Transient heat transfer effects on the pseudoelastic behavior of shape-memory wires”, *Acta Metall. Mater.* **41**:8 (1993), 2477–2485.
- [Liu et al. 1998] Y. Liu, Z. Xie, J. Van Humbeeck, and L. Delaey, “Asymmetry of stress-strain curves under tension and compression for NiTi shape memory alloys”, *Acta Mater.* **46**:12 (1998), 4325–4338.
- [Miyazaki et al. 1981] S. Miyazaki, T. Imai, K. Otsuka, and Y. Suzuki, “Lüders-like deformation observed in the transformation pseudoelasticity of a Ti–Ni alloy”, *Scr. Metall.* **15**:8 (1981), 853–856.
- [Otsuka and Wayman 1998] K. Otsuka and C. M. Wayman, *Shape memory materials*, Cambridge University Press, Cambridge, 1998.
- [Pieczyska et al. 2006a] E. A. Pieczyska, H. Tobushi, S. P. Gadaj, and W. K. Nowacki, “Superelastic deformation behaviors based on phase transformation bands in TiNi shape memory alloy”, *Mater. Trans. (JIM)* **47**:3 (2006), 670–676.
- [Pieczyska et al. 2006b] E. A. Pieczyska, H. Tobushi, S. P. Gadaj, and W. K. Nowacki, “Stress relaxation during superelastic behavior of TiNi shape memory alloy”, *Int. J. Appl. Electrom.* **23**:1–2 (2006), 3–8.

- [Raniecki and LExcellent 1998] B. Raniecki and C. LExcellent, “Thermodynamics of isotropic pseudoelasticity in shape memory alloys”, *Eur. J. Mech. A Solids* **17**:2 (1998), 185–205.
- [Saadat et al. 2002] S. Saadat, J. Salichs, M. Noori, Z. Hou, H. Davoodi, I. Bar-On, Y. Suzuki, and A. Masuda, “An overview of vibration and seismic applications of NiTi shape memory alloy”, *Smart Mater. Struct.* **11**:2 (2002), 218–229.
- [Shaw 2000] J. A. Shaw, “Simulations of localized thermo-mechanical behavior in a NiTi shape memory alloy”, *Int. J. Plast.* **16**:5 (2000), 541–562.
- [Shaw and Kyriakides 1995] J. A. Shaw and S. Kyriakides, “Thermomechanical aspects of NiTi”, *J. Mech. Phys. Solids* **43**:8 (1995), 1243–1281.
- [Shaw and Kyriakides 1997a] J. A. Shaw and S. Kyriakides, “On the nucleation and propagation of phase transformation fronts in a NiTi alloy”, *Acta Mater.* **45**:2 (1997), 683–700.
- [Shaw and Kyriakides 1997b] J. A. Shaw and S. Kyriakides, “Initiation and propagation of localized deformation elasto-plastic strips under uniaxial tension”, *Int. J. Plast.* **13**:10 (1997), 837–871.
- [Sittner et al. 2005] P. Sittner, Y. Liu, and V. Novak, “On the origin of Lüders-like deformation of NiTi shape memory alloys”, *J. Mech. Phys. Solids* **53**:8 (2005), 1719–1746.
- [Tan et al. 2004] G. Tan, Y. Liu, P. Sittner, and M. Saunders, “Lüders-like deformation associated with stress-induced martensitic transformation in NiTi”, *Scr. Mater.* **50**:2 (2004), 193–198.
- [Tanaka et al. 1986] K. Tanaka, S. Kobayashi, and Y. Sato, “Thermomechanics of transformation pseudoelasticity and shape memory effect in alloys”, *Int. J. Plasticity* **2**:1 (1986), 59–72.

Received 14 Oct 2007. Revised 17 Oct 2008. Accepted 24 Oct 2008.

B. AZADI BORUJENI: azadi@mech.ubc.ca

University of British Columbia, Department of Mechanical Engineering, 2054-6250 Applied Science Lane, Vancouver, BC 6T 1Z4, Canada

DAAN M. MAIJER: daan.maijer@ubc.ca

University of British Columbia, Department of Materials Engineering, 309-6350 Stores Road, Vancouver, BC V6T 1Z4, Canada

R. K. NIMAL D. RAJAPAKSE: rajapakse@mech.ubc.ca

University of British Columbia, Department of Mechanical Engineering, 2054-6250 Applied Science Lane, Vancouver, BC 6T 1Z4, Canada

